Dynamic Functional Connectivity in The Brain during Rhythm Listening: An fMRI Exploratory Study

Diana M. Urian

Department of Neuroscience, University of Western Ontario

Psychology 3997G: Independent Study

Author Note

This article was written for Psychology 3997G, to be completed by April 11, 2023. The described project was done as a continuation to the project started in Psychology 3996F. It was done under the direct supervision of Joshua Hoddinott and any pressing questions concerning this paper should be addressed to Dr. Jessica Grahn, principal investigator of the project and head of the Music and Neuroscience Lab (located on Perth Dr., London, ON, fifth floor of Western Interdisciplinary Research Building).

Table of Contents

Dynamic Functional Connectivity in The Brain during Rhythm Listening: An fMRI Exploratory Study

Precise timing plays a critical role in shaping behavior, facilitating learning, and governing sensorimotor processing. Achieving accurate timing requires intricate coordination between diverse neural subpopulations within forebrain circuits, specifically those encompassing the parietal and frontal cortices, basal ganglia, and cerebellum (Fontes et al., 2016). Auditory stimuli (e.g., from music) are among the many ways these circuits can be activated to enable the extraction of temporal regularities (Kotz et al., 2009). This is done through rhythm, which is a fundamental element in music that refers to the pattern of sounds and silences occurring over time. Rhythm is an important aspect of music since it creates structure that provides a sense of energy, movement, and emotion if the duration, accentuation, and placement of beats and silences is organized in a way to facilitate it (Sievers et al., 2013; Levitin et al., 2018). The study of rhythmic perception is a captivating field in the study of timing, as it plays a fundamental role in human auditory processing and is pivotal in comprehending music—an artform found in most cultures that provides cognitive, social, and emotional benefits. Research in this area can provide insight into the neural mechanisms involved in rhythm perception and how it may be impacted by speech-language pathology, motor disfunction, neurological disorders, or hearing impairments.

Nonetheless, the diverse and varied outcomes observed in functional magnetic resonance imaging (fMRI) investigations imply that the neural networks involved with rhythmic perception are intricate, underscoring the importance of proper imaging techniques to understand them. Three potential approaches may be considered, in order of increasing complexity: localized activity, static functional connectivity, or dynamic functional connectivity, each of which will be

described below. We will specifically focus on how these neuroimaging techniques can be used in rhythmic perception tasks, although they can be applied to various cognitive tasks.

The simplest approach to fMRI experiments, localized activity, evaluates blood-oxygen level-dependent (BOLD) brain activity to identify which anatomical regions of the brain are involved in a task, or process. This entails examining the activation patterns of various anatomical regions during a listening task and determining the degree to which they deviate from their baseline activation levels. It has been shown that temporal perception tasks, like rhythm listening, activate auditory regions (e.g., early sensory cortex regions, temporal lobe regions), as well as motor areas (e.g., supplementary motor area (SMA), basal ganglia, premotor cortex) (Kasdan et al., 2022). Specifically, the areas that activate seem to be dependent on whether there is the presence of a beat—the feeling of a steady pulse across a rhythm that allows a listener to tap along while listening. fMRI studies show that of all the rhythm-perception regions, the putamen and SMA activate more when individuals listen to rhythms with a strong-beat, compared to irregular, non-beat rhythms, suggesting that these regions may give rise to beat perception (Grahn & Brett, 2007; Grahn & Rowe, 2009).

Though motor regions appear to give rise to the beat, the beat arises from the rhythmic sounds in music, suggesting that there is likely some crosstalk between beat-perception regions and auditory regions when initially perceiving a beat. To address this issue, one may incorporate an additional level of complexity by analyzing the patterns of functional connectivity that persist throughout the scanning session. As in localized activity detection, functional connectivity measures the BOLD response. However, instead of testing for activity above a regional baseline, functional connectivity detects correlated activity *between* regions over a period of time, such as a task. Grahn and Rowe (2009) investigated static functional connectivity during beat perception.

Their findings demonstrated increased connectivity between the putamen and the bilateral SMA, premotor cortex (PMC), and auditory cortex when individuals were exposed to beat-based rhythms versus non-beat control rhythms. This led to the proposal of a cortico-subcortical network that includes crosstalk between the putamen, SMA, and PMC during beat perception.

All this considered, dynamic functional connectivity analysis can often offer even more captivating insights by utilizing a temporally-sensitive measure of functional connectivity. It is crucial to acknowledge that static functional connectivity analyses can solely capture consistent patterns of functional connectivity between different brain regions, which may stem from long-term anatomical connections or functional associations between these regions. Therefore, this approach may not be sufficient in estimating the complete spectrum of functional connectivity, given that brain connectivity is complex. Using static connectivity methods, we assume that the interdependence of signals between different areas in the brain is constant during rhythmic listening tasks, which may not be accurate as rhythm and beat may be especially prone to temporally-dependent brain activity. As stimuli are sequential, and inherently unfold over time, a rhythm cannot be perceived in one instant.

Current knowledge about the dynamic changes in functional connectivity over a rhythm is limited. However, previous research has distinguished between beat finding and beat continuation, suggesting potential time-dependent effects on rhythms. Beat finding (initial detection that a beat is present) occurs at the beginning of a beat rhythm, whereas beat continuation (prediction of future rhythmic events based on the preceding events) occurs whenever a rhythm continues at the same rate (Grahn & Rowe, 2013). A study done by Grahn and Rowe (2013) used fMRI to show that putamen activity facilitates prediction, but not detection; there is increased putamen activity when maintaining a beat across rhythms, compared

to initially detecting a beat. This study looked at localized activity however, and so our exploratory work aimed to investigate changes in dynamic functional connectivity in healthy individuals while perceiving rhythms. Specifically, we were interested in what would happen during longer rhythms since literature's use of short rhythms (~2-20 seconds) (Grahn & Rowe, 2013; Grahn and Rowe, 2009) may not accurately represent the longer rhythms typically encountered in musical contexts, which can be 120 seconds long or more.

We hypothesized that listening to a rhythm with a beat would lead to changes in temporal functional connectivity properties over time that would not be seen when the same individual listened to a non-beat rhythm or rest. This was based off research indicating that the presence of a beat significantly impacts how the brain processes stimuli. We utilized both dynamic functional connectivity and static functional connectivity analyses by extracting data from voxels within anatomically-defined regions of interest (ROIs) and restricted our analysis to ROI-ROI networks. Our study was the first attempt to explore the time-dependency of neural substrates during beat perception. The results supported the idea that brain networks undergo reorganization during different listening states, as evidenced by the changes in functional connectivity at various time points.

Method

Participants

The participants were students recruited from Western University, in London, Ontario, in 2015. Written informed consent was obtained from all participants. Twenty healthy individuals (eleven females, nine males; nineteen right-handed, one left-handed) with no history of neurological or psychiatric disorders participated in the functional connectivity MRI experiment. They ranged in age from 23 to 36 years (M = 25.5, SD = 4.1). The participants were screened for

inclusion criteria before admission to the experiment: no ferromagnetic material in their body; no implantable neurostimulation systems, no cochlear implants or hearing aids, no tattoos; no chronic pharmacological medication; no dopamine-driven psychotropic drugs, no claustrophobia (Dill, 2008). When measured on a scale from 1 (bad) to 6 (good), the participants reported adequate general hearing ability (M = 5.2, SD = 0.8). The participants also had variable levels of music experience, ranging from 0 to 23 years of playing (M = 7.9, SD = 6.4). When asked to report current hours of weekly practice, the average time spent was 0.9 hours (SD = 1.3). Although participants volunteered to participate, they were compensated $25/hour and the study was approved by the research ethics board at Western University.

Stimuli and Materials

Our research utilized pre-existing data that was generated in our laboratory for a cross-species investigation. The data was stored in our repository, from which it was subsequently repurposed to support the objectives of the current study.

Stimuli

Rhythmic stimuli were constructed using macaque calls to insure environmentally relevant stimuli for the animal model in the original study. The design of the stimuli was based on patterns described in a previous fMRI study (Grahn and Brett, 2007). There were three five-minute trials for each participant: a strong-beat condition (including a long, non-repeating strong-beat rhythm), a non-beat condition (including a long, non-repeating non-beat rhythm), and a resting-state condition (silent baseline).

In the strong-beat condition, the intervals in the rhythms were related by integer ratios of 1:2:3:4. The intervals were ordered such that they induced the perception of a regular beat; every four units started with a perceptually accented sound, corresponding to on-beat locations in a

duple meter (4/4) (Bouwer et al., 2018). A perceptual accent is an illusory emphasis that listeners tend to perceive on certain moments in a rhythm, based on the relative timing and duration of musical events (Povel & Essens, 1985). Accented intervals seem more salient (e.g., louder) even though physical properties are identical (Povel & Essens, 1985).

In the non-beat condition, the intervals in the rhythms were related by non-integer ratios, which disrupted any potential beat from being perceived in a rhythm. To create each non-beat stimuli, the duration of each interval making up the strong-beat exemplar was probabilistically adjusted by ±0% or 33%. These stimuli were made to mirror the strong-beat ones, rather than creating completely new rhythms. Intervals of length 1 were kept the same length or lengthened, intervals of length 2 or 3 were shortened, kept the same or lengthened, and intervals of length 4 were shortened or kept the same length.

Materials

Procedure. Participants were placed in an fMRI scanner and asked to stay still to control for the over-activation of cerebral motor areas. Participants were exposed to one of three experimental conditions during the initial five-minute period. The study employed separate fMRI scans to assess participants' responses to strong-beat rhythm, non-beat rhythm, and silence, with counterbalancing across participants to mitigate any potential order effects. This approach helped to minimize the likelihood of carry-over effects from the listening experience and any demand characteristics. Specifically, if the strong-beat condition always came before the non-beat condition, participants might have been more likely to detect differences between the conditions, thereby confounding the results. Similarly, if the non-beat always preceded the strong-beat, participants might have immediately become aware of the presence of a beat, potentially altering the speed with which they detect and maintain it. Furthermore, it is worth noting that potential

fatigue effects may have arisen during the latter scan runs, as participants would have been approximately ten minutes into the scanning session by that point.

Apparatus. Scanning was performed using a MAGNETOM 7T Siemens whole-body fMRI scanner at the Center for Functional and Metabolic Mapping in the Robarts Research Institute (Western University, London, Canada). Using an interleaved echo planar imaging (EPI) sequence, 48 slices (field of view: 220 mm x 220 mm; slice thickness: 4 mm; TR: 1250 ms: TE: 20 ms; flip angle: 35; voxel size: 2.5 x 2.5 mm, with a slice thickness of 2.5 mm; multiband acceleration factor: 2) were acquired every 1.25 s, providing a whole-brain coverage per participant. T1-weighted sagittal anatomical images (208 slices per slab; field of view: 240 x 240 mm; slice thickness: 0.80 x 0.80 mm; pulse sequence: MPRAGE; TR: 6000; TE: 1.94 ms) were also collected for each individual.

Preprocessing

Data preprocessing was carried out using Statistical Parametric Mapping (SPM) software (RRID:SCR_007037) v.12 implemented in MATLAB (version R2023a, MathWorks, Inc., Natick, MA, USA). To address interscan head motions and misalignments in functional images, the data were realigned to the first volume. Next, they were coregistered, segmented into grey matter, white matter, and CSF using the Tissue Probability Map template, and normalized into the standard Montreal Neurological Institute space via non-linear transformations. Additionally, a Gaussian smoothing kernel with a 6 mm full-width at half-maximum was employed to enhance the signal and reduce noise.

Denoising

The functional data was processed to remove any noise using a commonly used method known as denoising pipeline using CONN (RRID:SCR_009550) release 22.a. Denoising fMRI

data is necessary to minimize physiological noise, and motion and scanner artifacts. Our denoising specifically focused on accounting for motion parameters, outlier scans, session and task effects, and white matter and cerebrospinal fluid timeseries. Eliminating any physiological correlations (e.g., areas driven by cerebrospinal fluid) and center connectivity values on zero is important, so that if two areas are correlated just due to anatomical artifacts, no false positives are created. After this, the data was filtered to only include frequencies between 0.01 Hz and 0.1 Hz, which are believed to be most relevant for studying brain activity. Overall, denoising the fMRI data in this way was crucial to increase the signal-to-noise ratio (SNR), and therefore the reliability of our results.

Regions of Interest

Using the Harvard-Oxford Cortical and Subcortical atlas loaded into CONN, we extracted signals from the following anatomically-defined ROIs: the right supplementary motor area (SMA) near (6, -3, 58) mm, the left SMA near (-5, -3, 56) mm; the right posterior superior temporal gyrus (pSTG) near (61, -24, 2) mm, the left pSTG near (-62, -29, 4) mm; the right putamen near (25, 2, 0) mm; and, the left putamen near (-25, 0, 0). We chose to focus on ROI analysis, as opposed to seed-based (i.e., whole-brain) analysis, given that prior research has identified these specific ROIs as being activated during auditory tasks and rhythm perception. This decision was also motivated by the need to minimize the risk of committing Type I errors; this type of analysis limits the number of statistical tests to a few ROIs (Poldrack, 2007). These regions were then analyzed with first-level and second-level analysis.

First-level Analysis

First-level analysis was performed using CONN (RRID:SCR_009550) v.22. Functional connectivity strength was represented by Fisher-transformed bivariate correlation coefficients

from a weighted general linear model (weighted-GLM), defined separately for each pair of ROI target areas. This was done to correlate the BOLD signal timeseries within each subject, and condition. The sole distinguishing factor between static and dynamic first-level analysis was the incorporation of nine overlapping time windows into the weighted-GLM of the latter.

To create the dynamic time windows, we used a Sliding Window Analysis in CONN. This technique divides the imaging time series into multiple smaller, overlapping bins (i.e., "windows") that can be compared. The functional connectivity is measured separately within each window and there is a succession of pairwise correlation matrices using the time series from the ROIs to determine whether, or how, connectivity changes over time (Mokhtari et al., 2019). The CONN default sliding window parameters were used: windows of 100-second duration, with window onsets occurring every 25 seconds (i.e., the onset of the subsequent window occurs 25 seconds following the onset of the preceding window). Since our stimuli were 300 seconds (five minutes), this resulted in nine 100-second-long time windows.

Second-level Analysis

To analyze the data at the group level, CONN was also utilized. We extracted the data from the first-level analysis to draw conclusions regarding the entire population from which the sample was obtained. The connectivity values for static and dynamic functional connectivity were then independently analyzed for each ROI pair. We tested the static functional connectivity using a one-way ANOVA in CONN and looked for any effects (i.e., region-to-region connectivity within each condition) or any differences (i.e., region-to-region connectivity that differed between conditions). This test accounted for the multiple comparisons we made by using the false discovery rate (FDR) correction. We tested the dynamic functional connectivity using a repeated-measures two-way ANOVA in Jeffrey's Amazing Statistics Program (JASP).

Results

Static Functional Connectivity

As a preliminary step, we examined the presence of static functional connectivity across the entire presentation of the stimuli. This part of the analysis involved comparing the ROI-ROI connectivity correlations across all time points of the strong-beat, non-beat, and silence conditions. The functional connectivity analysis revealed that almost all ROI pairs exhibited significant functional connectivity during strong-beat conditions, as determined by the average correlation values across all time windows (Table 1). The only regions that did not show significant functional connectivity included the right pSTG and left putamen, and left pSTG and right putamen. When it came to the non-beat condition (Table 2), all areas showed significant connectivity except the pSTG and putamen ROI pairs (right pSTG and right putamen, right pSTG and left putamen, left pSTG and right putamen, and left pSTG and left putamen). Similarly, during silence (Table 3), all the pSTG and putamen ROI pairs were non-significant, in addition to most of the SMA and pSTG pairs (right SMA and left pSTG, left SMA and right pSTG, and left SMA and left pSTG). The other ROI pairs during silence showed significance. In general, it appeared that functional connectivity between regions was consistently present across all conditions, except when examining the connectivity between the pSTG and putamen, or pSTG and SMA.

Subsequently, we aimed to examine whether variations in functional connectivity existed among the ROI pairs across the three distinct listening conditions. A repeated measures one-way analysis of variance (ANOVA) was conducted for each ROI pair, using CONN. This revealed no significant difference in functional connectivity between the three different listening conditions (shown in Table 4). There was marginal significance seen between the left SMA and the left

putamen, but overall, we concluded that there was no significant effect of stimulus type on the static functional connectivity between our ROI pairs.

However, although no statistical significance was established, visual inspection of the general connectivity differences between the conditions revealed interesting findings. Using CONN output graphs (i.e., the connectivity model effects seen on the REX interface), we detected that the functional connectivity between the left SMA and right pSTG exhibited variability between conditions: silence showed the lowest connectivity, non-beat showed moderate connectivity, and strong-beat showed the highest connectivity. Similar effects were seen between the right SMA and right pSTG, the right SMA and left pSTG, and the left pSTG and left putamen. That is, the functional connectivity within these pairs of areas were weaker during silence, moderate during weak-beat, and strongest during strong-beat conditions. Conversely, a contrasting trend emerged with respect to the connectivity patterns between the left SMA and the right putamen: the strong-beat condition appeared to elicit lower levels of functional connectivity when compared to both the non-beat and silence conditions. This last observance explained the marginal significance in the previous step involving the comparison of static functional connectivity between different conditions.

The lack of statistical support for differences in functional connectivity among the three different stimuli conditions bears both favorable and unfavorable implications. It is unfavourable given that past literature led us to anticipate greater functional connectivity between specific regions during the strong beat condition, such as the SMA and putamen (Grahn & Rowe, 2013). On the other hand, this outcome is favourable because it makes the question of dynamic functional connectivity even more intriguing. It is plausible that temporal variations exist, but they remain concealed by static functional connectivity analysis which takes an entire 300-

second stimulus into account. The rhythmic stimuli could potentially result in substantial differences in connectivity patterns during distinct time points within the stimuli presentation, which static connectivity cannot detect.

Dynamic Functional Connectivity

Static connectivity analysis did not replicate prior research findings, leading to the possibility that functional connectivity may exist only during certain time intervals within a rhythm. To investigate this further, we aimed to identify variations in correlation time series across different windows and listening conditions in one singular analysis. Our goal was to discern whether fluctuations in the correlation time series were distinguishable from those expected under static correlation (i.e., independent of time) between the different windows and listening conditions.

If there was a greater extent of overall connectivity within a specific auditory condition (e.g., stronger connectivity in the strong-beat condition versus the non-beat condition), a main effect of stimulus condition would have been observed. Should all stimulus conditions have displayed similar alterations in connectivity over time, a significant effect of time would have been observed. Conversely, if changes in connectivity over time were solely observed within one or more auditory conditions, an interaction would have been observed. Based on Grahn and Rowe's (2013) findings, we posited that an interaction effect would be evident.

We performed a two-way repeated measures ANOVA for each ROI pair using JASP. This was done to compare the effect of both stimulus and time on functional connectivity, as measured by Fisher-transformed bivariate correlation coefficients (3 x 9 analysis; (strong-beat, non-beat, silence) x (time 1-time 9)). Our analysis resulted in 15 independent repeated measures ANOVAs, which revealed no significant main effects for either stimulus or time across any of

the ROI pairs (shown in Table 5). However, in alignment with our initial hypothesis, interactions were observed. Our analysis revealed that four ROI pairs exhibited significant stimulus condition x time interactions: the right pSTG and right putamen, the right pSTG and left putamen; the right pSTG and left pSTG; and the left SMA and left putamen. We will discuss significant t-test results from each ROI pair that yielded significance. Insignificant t-tests from these ROI pairs will be presented in corresponding tables at the end for reference. As we did not use FDR correction to account for multiple corrections, there is a possibility of false positives due to the implementation of 15 separate ANOVAs. Therefore, our findings should be viewed with caution.

Right pSTG and right putamen. Starting with the right pSTG and right putamen, a two-way ANOVA revealed that neither stimulus ($F_{2,38} = 0.10$, $p = 0.905$), nor time ($F_{8,152} = 1.08$, $p = 0.380$), significantly affected functional connectivity between these regions, but that there was a statistically significant interaction between the effects of stimulus and time ($F_{16,304} = 3.11$, $p < .001$). We followed up this interaction with post-hoc t-tests using custom MATLAB code (results shown in Table 9). There were significant differences across all three stimuli conditions during the first, second, and third time windows. During the first time window, strong-beat functional connectivity ($M = 0.21$, $SD = 0.29$) was significantly greater compared to non-beat functional connectivity ($M = 0.02$, $SD = 0.34$) ($t(19) = 2.15$, $p = 0.045$) and silence functional connectivity ($M = 0.03$, $SD = 0.24$) ($t(19) = 2.76$, $p = 0.013$). There was no significant difference in connectivity between non-beat and silence during this window ($t(19) = -0.08$, $p = 0.941$). During the second time window, strong-beat functional connectivity ($M = 0.24$, $SD = 0.25$) was significantly greater compared to non-beat functional connectivity ($M = 0.06$, $SD = 0.29$) ($t(19) = 2.36$, $p = 0.013$) and silence functional connectivity ($M = 0.03$, $SD = 0.20$) ($t(19)$

= 2.15, p = 0.004). There was no significant difference in the connectivity between non-beat and silence during this window ($t(19) = 0.33$, $p = 0.745$).

We also identified three distinct time windows that exhibited significant differences in connectivity, albeit only when comparing between two specific conditions. During the third time window, strong-beat functional connectivity ($M = 0.18$, $SD = 0.27$) was significantly greater compared to silence functional connectivity ($M = 0.03$, $SD = 0.20$) ($t(19) = 2.23$, $p = 0.038$). During the sixth time window, strong-beat functional connectivity ($M = 0.01$, $SD = 0.17$) was significantly lower compared to non-beat functional connectivity ($M = 0.16$, $SD = 0.30$) ($t(19) = -2.36$, $p = 0.029$). Finally, during the eighth time window, strong-beat functional connectivity ($M = -0.08$, $SD = 0.311$) was significantly lower compared to silence functional connectivity ($M = 0.12$, $SD = 0.24$) ($t(19) = -2.10$, $p = 0.050$). The t-tests comparing connectivity between other stimuli condition combinations for the third, sixth, and eighth windows were not significant ($p > .05$, Table 9), and thus, no definitive conclusions can be drawn regarding general patterns across conditions for these time windows.

Overall, this post-hoc analysis suggested that the connectivity between right pSTG and right putamen was significantly greater towards the beginning of the five-minute block when a strong-beat rhythm was playing, compared to non-beat and silence conditions (Figure 5).

Right pSTG and left putamen. The next regions to analyze were the right pSTG and left putamen. A two-way ANOVA similarly revealed that neither stimulus ($F_{2,38} = 1.69$, $p = 0.198$), nor time ($F_{8,152} = 0.58$, $p = 0.790$), significantly affected functional connectivity between these regions, but that there was a statistically significant interaction between the effects of stimulus and time ($F_{16,304} = 2.15$, $p = 0.007$). Post-hoc t-tests (results shown in Table 7) revealed that in the fourth time window, silence functional connectivity ($M = -0.10$, $SD = 0.31$) was significantly

lower (negative), compared to strong-beat functional connectivity (M = 0.10, SD = 0.24) ($t(19)$ = 2.39, p = 0.028) and non-beat functional connectivity (M = 0.08, SD = 0.23) ($t(19)$ = 2.66, p = 0.016). There was no significant difference in the connectivity between strong-beat and non-beat during this window ($t(19)$ = 0.53, p = 0.606).

We also identified two distinct time windows that exhibited significant differences in connectivity, albeit only when comparing between two specific conditions. During the second time window, strong-beat functional connectivity (M = 0.17, SD = 0.27) was significantly greater compared to silence functional connectivity (M = -0.04, SD = 0.27) ($t(19)$ = 2.23, p = 0.038), and during the third time window, non-beat functional connectivity (M = 0.12; SD = 0.23) was significantly greater compared to silence functional connectivity (M = -0.07, SD = 0.27) ($t(19)$ = 2.57, p = 0.019). The t-tests comparing connectivity between other stimulus condition combinations for the second and third windows were not significant ($p > .05$), and thus, no definitive conclusions can be drawn regarding general patterns across conditions for these time windows.

Overall, this post-hoc analysis suggested that the connectivity between the between left putamen and right pSTG was significantly lower towards the middle of the five-minute block during silence, compared to when a rhythm was playing (either strong- or non-beat) (Figure 3).

Right pSTG and left pSTG. When looking at the functional connectivity between the right pSTG and left pSTG, a two-way ANOVA similarly revealed no stimulus main effect ($F_{2,38}$ = 1.16, p = 0.323), nor time main effect ($F_{8,152}$ = 1.15, p = 0.332), with a statistically significant interaction between the effects of stimulus and time ($F_{16,304}$ = 3.02, $p < .001$). Post-hoc t-tests found that there were significant differences across all three stimuli conditions during the second and third interval of listening to the stimuli (results shown in Table 8). In the second time

window, silence functional connectivity ($M = 0.50$, $SD = 0.38$) was significantly lower compared to strong-beat functional connectivity ($M = 0.78$, $SD = 0.35$) ($t(19) = 2.35$, $p = 0.030$) and non-beat functional connectivity ($M = 0.72$, $SD = 0.36$) ($t(19) = 2.53$, $p = 0.020$). There was no significant difference in the connectivity between strong-beat and non-beat during this window ($t(19) = 0.62$, $p = 0.541$). In the third window, silence functional connectivity ($M = 0.60$, $SD = 0.39$) was similarly significantly lower compared to strong-beat functional connectivity ($M = 0.83$, $SD = 0.39$) ($t(19) = 2.42$, $p = 0.026$) and non-beat functional connectivity ($M = 0.77$, $SD = 0.44$) ($t(19) = 3.13$, $p = 0.006$). There was no significant difference in the connectivity between strong-beat and non-beat during this window either ($t(19) = -0.21$, $p = 0.833$).

Overall, this post-hoc analysis suggests that the connectivity between the left pSTG and right pSTG was significantly greater towards the start of the five-minute block when a rhythm was playing (either strong- or non-beat), compared to silence (Figure 4).

Left SMA and left putamen. Finally, a two-way ANOVA revealed that neither stimulus ($F_{2,38} = 2.53$, $p = 0.093$), nor time ($F_{8,152} = 0.57$, $p = 0.802$), significantly affected functional connectivity between the left SMA and left putamen, but that there was a statistically significant interaction between the effects of stimulus and time ($F_{16,304} = 2.49$, $p = 0.001$). A post-hoc t-test (results shown in Table 6) analysis revealed that in the eight time window, strong-beat functional connectivity ($M = 0.09$, $SD = 0.36$) was significantly lower compared to non-beat functional connectivity ($M = 0.31$, $SD = 0.25$) ($t(19) = -2.16$, $p = 0.043$) and silence functional connectivity ($M = 0.40$, $SD = 0.33$) ($t(19) = -3.08$, $p = 0.006$). There was no significant difference in the connectivity between non-beat and silence during this window ($t(19) = -1.13$, $p = 0.274$).

We also identified four distinct time windows that exhibited significant differences in connectivity, albeit only when comparing between two specific conditions. During the sixth time

window, strong-beat functional connectivity (M = 0.19, SD = 0.29) was significantly lower compared to silence functional connectivity (M = 0.37, SD = 0.23) ($t(19) = -3.48$, $p = 0.003$). During the seventh time window, strong-beat functional connectivity (M = 0.17, SD = 0.31) was significantly lower compared to silence functional connectivity (M = 0.39, SD = 0.26) ($t(19) = -3.22$, $p = 0.005$). During the eighth time window, strong-beat functional connectivity (M = 0.09, SD = 0.36) was significantly lower compared to silence functional connectivity (M = 0.40, SD = 0.33) ($t(19) = -3.08$, $p = 0.006$). During the ninth time window, strong-beat functional connectivity (M = 0.12, SD = 0.33) was significantly lower compared to silence functional connectivity (M = 0.39, SD = 0.28) ($t(19) = -2.94$, $p = 0.008$). The t-tests comparing connectivity between other stimulus condition combinations for the sixth, seventh, eighth, and ninth windows were not significant ($p > .05$), and thus, no definitive conclusions can be drawn regarding general patterns across conditions for these time windows.

Overall, this post-hoc analysis suggests that the connectivity between the left SMA and left putamen was significantly lower towards the end of the five-minute block when a strong-beat rhythm was playing, compared to non-beat rhythms or silence (Figure 2).

Other ROI pairs. Two-way ANOVAs revealed that that neither stimulus, nor time, had a statistically significant effect on functional connectivity between all of the other ROI pairs, and there was no statistically significant interaction between the effects of stimulus and time (shown in Table 5).

Discussion

In the past, static connectivity demonstrated that both auditory and motor areas are involved with beat perception, but failed to address whether this fluctuates over the course of a long rhythm. Our current study investigated this relationship by specifically looking into the

right and left SMA (motor regions), the right and left pSTG (auditory regions), and the right and left putamen (motor and timing regions). To the best of our knowledge, we were the first to investigate dynamic functional connectivity in this area of research.

Data Interpretation

Simply observing the fluctuations through the general shapes of correlation over time revealed why certain regions initially showed no significant static connectivity (shown in Figure 1). When looking at the curve for the right pSTG and left putamen (Figure 3), for example, each listening condition showed to have fluctuations that would approximately be around zero if averaged. This explained why we detected there to be no static connectivity between these regions within any condition. This also highlighted why the regions did not exhibit any significant differences between conditions during the static functional connectivity analysis; when values fluctuate around a constant value, regardless of the shape of the fluctuation, they appear indistinguishable from one another. Dynamic functional connectivity analysis became vital as it enabled the identification of subtle differences that static functional connectivity failed to capture. In fact, our dynamic functional connectivity analysis revealed temporal variations in the functional connectivity between the left putamen and right pSTG across different conditions. We also observed that the right pSTG and right putamen connectivity had a significant temporal dependence across conditions, even though the static functional connectivity initially showed neither functional connectivity in these ROI pairs, nor differences between listening conditions.

In the context of dynamic functional connectivity analysis, we observed that among all the conceivable ROI pairs, the pSTG was implicated in three out of the four regions that exhibited significant results. When there is auditory stimulation, more connectivity generally is seen within this region (strong-beat and non-beat > silence), making this observation reasonable.

An interesting finding was that the right pSTG and right putamen had higher connectivity during the beginning of strong-beat conditions (Figure 5). It seems that the putamen and STG communicate during rhythms that contain a strong-beat rhythm, but only early in the listening task. We know from past research that the putamen is needed to detect a beat in the first moments of a rhythm, but it's possible that it doesn't continue the beat on its own if the stimuli presentations are long. Cannon & Patel (2021) describe a model in which they suggest that the putamen and SMA inform auditory regions when to expect sounds. Thus, it is possible that once the expectation is setup, the connection doesn't need to be as strong, decaying connectivity over time. The pSTG may exhibit a strong connection with the putamen at the start of a beat-containing rhythm, which gradually diminishes as the rhythm unfolds and becomes more familiar. Once the putamen detects the beat and transmits it to the pSTG for encoding, it is plausible that the pSTG independently sustains the beat. Although this hypothesis lacks empirical support, it remains a potential avenue for future research. Conversely, in the case of non-beat rhythms, they are difficult to predict, so even later in the rhythm the putamen may be updating predictions and thus continue to be functionally connected to STG. That is, in the absence of an auditory stimulus, a corresponding reduction in pSTG-putamen connectivity is not observed since the putamen fails to initiate the beat, precluding the pSTG from taking over.

This concept might explain the significant increase in functional connectivity between the right and left pSTG shortly after the start of the stimulus presentation (time window two and three) while listening to auditory stimuli (strong- and non-beat rhythms) but not during silence (Figure 4). The observed increase in STG-STG connectivity (hemispheric crosstalk) during the beginning of the rhythm is consistent with the possibility that the pSTG is primed to integrate, and store, the temporal information provided by the putamen at the trial's outset, regardless of

whether a beat is present. In the absence of auditory input (silence), the pSTG may attempt to encode information to generate predictions but ultimately fail, rendering sustained hemispheric crosstalk unnecessary.

Further supporting this idea is that toward the end of a listening block, there was lower functional connectivity seen between the right pSTG and left putamen in the strong-beat condition, compared to non-beat and silence conditions. The lends support to the notion that strong-beat rhythms, once established, exhibit a high degree of predictability and consequently require diminished input from the putamen to the pSTG. Specifically, during the beat, the putamen serves to impart temporal information to the pSTG until the latter assumes the dominant role, culminating in an observable shift in functional connectivity between the two brain regions. In contrast, when a non-beat is present, the putamen cannot provide enough temporal information to sustain the internal feeling of the beat, leading to relatively stable connectivity between the putamen and pSTG across time windows (Figure 3).

Alternatively, a decrease in connectivity between these regions could suggest disengagement and reduced attention to the beat. However, this explanation seems less plausible since we would expect general decreases in non-beat conditions too as time progresses. While the present findings provide a promising starting point, further research is needed to validate our theoretical postulations.

Finally, we found significantly lower connectivity between the right pSTG and left putamen during silence, compared to auditory stimuli (strong- and non-beat rhythms) in the fourth time window. The silent condition was added to characterize how two regions are naturally connected over time, accounting for the effects of being in an fMRI scanner (which in

itself is a loud acoustic environment). Thus, the large variability in connectivity across time in the silence condition is interesting, but difficult to interpret.

Limitations and Future Directions

Our study suffers from several limitations. Generally, an fMRI study requires a minimum of 25 participants to achieve adequate power. It is possible that the data collected from our small sample of 20 participants do not fully reflect the broader patterns of human behavior. However, it is worth noting that despite our small sample size, there was a degree of consistency in our significant findings, providing us with a basis for our theoretical interpretation and implying that chance may not be the sole explanation. Another factor to consider is the potential confounding effect of attention on our results, as participants were not engaged in any specific task during the scanning. Enduring prolonged periods of listening to macaque calls while remaining stationary is a challenging task for participants due to the monotonous nature of the activity, coupled with the unfamiliarity of the sounds in comparison to what they are accustomed to hearing.

All this said, exploratory studies rarely provide definitive answers to research questions, only offering direction for further research methods. As such, with the initial findings our study, there is much room for further investigation. For instance, a seed-based analysis could be employed to explore potential changes in brain regions beyond those selected as our ROIs. This approach would allow for a more comprehensive examination of the neural mechanisms involved in rhythm perception, potentially revealing unexpected brain regions involved in this process. Prior studies have suggested that other cognitive functions, such as memory, may be altered following musical listening tasks, suggesting the possibility of a greater extent of neural connectivity in the brain than has been previously assumed (Simmons-Stern et al., 2012). Although memory regions have not frequently been observed in fMRI scans during beat

perception tasks, this may be due to the rapid and dynamic temporal changes that occur during these tasks. If this is the case, the fluctuations in connectivity between these regions would be missed by static functional connectivity analysis and would best be detected on a whole-brain dynamic functional connectivity analysis.

Additionally, an important avenue for future research would be to investigate the phenomenon of lateralization. Visual inspection (Figure 1) led us to suspect the possibility of lateralized inter-regional connectivity, which is notable given that previous research has established that the brain usually engages both hemispheres during rhythm processing. Specifically, we found that the dynamic functional connectivity between the right pSTG and right putamen (Figure 5) exhibited similar trends as that between the right pSTG and left putamen (Figure 3). That is, for both putamen regions, the strong-beat condition led to decreases in functional connectivity across time windows and relatively stable functional connectivity within the non-beat condition. We then noted that the way the left pSTG dynamically connected to the putamen differed from that seen in the right pSTG. However, the left pSTG connections to the right and left putamen exhibited similar trends (i.e., the strong-beat and non-beat conditions lines appeared to follow the same trend). Thus, it appears that while the left and right pSTG contribute to beat perception in different ways while an individual perceives a rhythm, each individually communicates in a specific manner with both the left and right putamen. This suggests that there may be functional lateralization in the superior temporal gyrus. While there is limited research on the topic, prior studies have indicated that asymmetries in the functional and morphological aspects of the temporal lobe occur naturally during development, thus implying the possibility of lateralization in the pSTG (Bisiacchi & Cainelli, 2022).

We could also consider shortening the window to see finer time-scales and improve our temporal resolution (Hindriks et al., 2016). The selection of an appropriate window size is a crucial aspect when employing a Sliding Window paradigm. It is desirable for the window to be large enough to facilitate accurate estimation of functional connectivity and to detect the lowest frequencies of interest within the signal, while simultaneously small enough to detect potentially meaningful transients (Hutchison et al., 2013). Typically, window sizes ranging from 30-60 seconds have been shown to produce robust results (Hutchison et al., 2013). Since our window sizes were notably larger than this range, one might consider shrinking the window size. However, as one does so, the SNR of the estimated BOLD functional connectivity signal decreases and the overall variability in functional connectivity tends to increase (Hutchison et al., 2013). As such, to combat this and still address the sizing problem, one might consider multi-scale approaches (Hutchison et al., 2013). These approaches analyze data at multiple time scales by utilizing varying window sizes, thereby enhancing the sensitivity to detect connectivity changes that occur at different temporal scales (Hutchison et al., 2013). The multi-scale approach adjusts the window size to match the inherent time-scale of how signals change in network connectivity. Shorter time windows are used to analyze high frequency connectivity changes, while longer time windows are used to analyze lower frequency connectivity changes (Hutchison et al., 2013). Our sliding window technique employed a fixed window size and may not be as effective in detecting changes in connectivity across the entire temporal range.

Alternatively, instead of the time window multi-scale approachs, we could do a regression analysis. In our visual inspections (Figure 1), we noted that the changes in functional connectivity exhibited varied patterns, including linear and non-linear components. It would be worthwhile to investigate whether a specific mathematical function can accurately capture the

dynamic changes in functional connectivity within specific regions during exposure to strong-beat rhythms. Future research could conduct a regression analysis using different functions as predictors, such as quadratic and linear functions, to identify any underlying patterns. This approach may provide a more comprehensive understanding of the temporal changes in functional connectivity compared to the current method of analyzing individual windows.

Moreover, it would be intriguing to investigate the dynamic connectivity during a weak-beat condition, which corresponds to a moderate level of perceived rhythmicity. If data on weak-beat rhythms were available and functional connectivity trends could be identified with amplitudes that generally average those of the strong- and non-beat conditions, our conclusions would have been further strengthened. Nevertheless, this limitation can benefit exploratory research by minimizing the number of variables, facilitating clearer interpretation of results. By working with only strong-beat and non-beat conditions, which are very distinct rhythmic stimuli, our conclusions were easier to interpret. Additionally, it should be noted that the original researchers may have intentionally omitted this stimulus type to reduce the fMRI scanning time for participants.

Another aspect that merits consideration pertains to the use of naturalistic musical rhythms, which are more complex and holistic than the macaque calls utilized in this study. The primary motivation behind our investigation into the neural mechanisms underlying rhythm perception and processing is to comprehend the effects of listening to music on the brain. By incorporating songs and other elements that constitute music (e.g., melody and harmony), we may increase the external validity of our findings.

Our long-term objective, albeit ambitious, is to apply this knowledge to clinical settings. Thus, if we can identify temporal disparities in dynamic functional connectivity during exposure

to specific rhythms, the next step would be to measure the impact of compromised systems. For example, testing patients with Parkinson's disease, who suffer from disrupted basal ganglia activity, may reveal whether dynamic changes in functional connectivity are absent, altered, or unchanged while listening to long rhythms. Such information could potentially transform how we approach and develop music therapy programs.

The differential engagement of brain networks associated with motor control and coordination during distinct phases of rhythmic stimuli also holds potential for applications in movement disorder and stroke rehabilitation (Janzen et al., 2022). For instance, if a replication study finds that the activation of movement networks (e.g., involving the basal ganglia) is found to be maximal at the onset of an auditory stimulus, rhythmic auditory stimulation can selectively target and activate these neural networks, through short segments of music. It may not be necessary to utilize extended musical pieces during therapy when only the initial moments of rhythmic stimulation are needed to activate the relevant brain regions. Additionally, it might be beneficial to consider switching songs more often to make people perceive beats frequently.

Conclusion

All this considered, this research marks an important initial step towards a more comprehensive understanding of beat perception, offering valuable insights into the underlying networks involved. The exploratory nature of this study has enabled the emergence of new ideas in this field through a data-driven analysis, without the limitations of hypothesis-driven work. The observed significant differences in dynamic functional connectivity between distinct listening conditions, despite the modest sample size, suggest the potential usefulness of this method. However, the application of such research is contingent on future replication efforts. To

advance this field of research, it is recommended that future studies improve the quality of stimuli and consider the limitations and potential areas for future exploration mentioned above.

References

Bisiacchi, P., & Cainelli, E. (2022). Structural and functional brain asymmetries in the early phases of life: A scoping review. *Brain Structure and Function, 227*(2), 479–496. https://doi.org/10.1007/s00429-021-02256-1

Cannon, J. J., & Patel, A. D. (2021). How beat perception co-opts motor neurophysiology. *Trends in Cognitive Sciences, 25*(2), 137-150. https://doi.org/10.1016/j.tics.2020.11.002

Dill, T. (2008). Contraindications to magnetic resonance imaging. *Heart (British Cardiac Society), 94*(7), 943–948. https://doi.org/10.1136/hrt.2007.125039

Grahn, J. A., & Brett, M. (2007). Rhythm and beat perception in motor areas of the brain. *Journal of Cognitive Neuroscience, 19*(5), 893–906. https://doi.org/10.1162/jocn.2007.19.5.893

Grahn J. A., & Rowe, J. B. (2009). Feeling the beat: Premotor and striatal interactions in musicians and nonmusicians during beat perception. *The Journal of Neuroscience, 29*(23), 7540–7548. https://doi.org/10.1523/JNEUROSCI.2018-08.2009

Grahn J. A., & Rowe, J. B. (2013). Finding and feeling the musical beat: Striatal dissociations between detection and prediction of regularity. *Cerebral Cortex, 23*(4), 913–921. https://doi.org/10.1093/cercor/bhs083

Hindriks, R., Adhikari, M. H., Murayama, Y., Ganzetti, M., Mantini, D., Logothetis, N. K., & Deco, G. (2016). Can sliding-window correlations reveal dynamic functional connectivity in resting-state fMRI? *NeuroImage, 127*, 242–256. https://doi.org/10.1016/j.neuroimage.2015.11.055

Hutchison, R. M., Womelsdorf, T., Allen, E. A., Bandettini, P. A., Calhoun, V. D., Corbetta, M., Penna, S. D., Duyn, J. H., Glover, G. H., Gonzalez-Castillo, J., Handwerker, D. A., Keilholz, S., Kiviniemi, V., Leopold, D. A., de Pasquale, F., Sporns, O., Walter, M., & Chang, C. (2013). Dynamic functional connectivity: Promise, issues, and interpretations. *NeuroImage, 80*, 10.1016/j.neuroimage.2013.05.079. https://doi.org/10.1016/j.neuroimage.2013.05.079

Janzen, B. T., Koshimori, Y., Richard, N. M., & Thaut, M. H. (2022). Rhythm and music-based interventions in motor rehabilitation: Current evidence and future perspectives. *Frontiers in Human Neuroscience, 15*. https://www.frontiersin.org/articles/10.3389/fnhum.2021.789467

Levitin, D. J., Grahn, J. A., & London, J. (2018). The Psychology of music: Rhythm and movement. *Annual Review of Psychology, 69*(1), 51–75. https://doi.org/10.1146/annurev-psych-122216-011740

Mokhtari, F., Akhlaghi, M. I., Simpson, S. L., Wu, G., & Laurienti, P. J. (2019). Sliding window correlation analysis: Modulating window shape for dynamic brain connectivity in resting state. *NeuroImage, 189*, 655–666. https://doi.org/10.1016/j.neuroimage.2019.02.001

Poldrack, R. A. (2007). Region of interest analysis for fMRI. *Social Cognitive and Affective Neuroscience, 2*(1), 67–70. https://doi.org/10.1093/scan/nsm006

Povel, D. J., & Essens, P. (1985). Perception of temporal patterns. *Music Perception, 2*(4), 411-440. https://doi.org/10.2307/40285311

Sievers, B., Polansky, L., Casey, M., & Wheatley, T. (2013). Music and movement share a dynamic structure that supports universal expressions of emotion. *Proceedings of the National Academy of Sciences, 110*(1), 70–75. https://doi.org/10.1073/pnas.1209023110

Simmons-Stern, N. R., Deason, R. G., Brandler, B. J., Frustace, B. S., O'Connor, M. K., Ally, B. A., & Budson, A. E. (2012). Music-based memory enhancement in Alzheimer's Disease: Promise and limitations. *Neuropsychologia, 50*(14), 3295–3303. https://doi.org/10.1016/j.neuropsychologia.2012.09.019

Tables

Table 1

ANOVA Results for Static Connectivity during Strong-Beat Rhythms in Various Brain Regions

ROI pair	$F_{1,19}$	*p*-FDR
Right SMA-left SMA**	303.56	< .001
Right SMA-right pSTG**	21.60	< .001
Right SMA-left pSTG**	15.17	0.001
Right SMA-right putamen**	19.10	< .001
Right SMA-left putamen**	13.72	0.002
Left SMA-right pSTG**	24.96	< .001
Left SMA-left pSTG**	10.44	0.004
Left SMA-right putamen**	18.86	< .001
Left SMA-left putamen**	10.93	0.004
Right pSTG-left pSTG**	106.73	< .001
Right pSTG-right putamen*	6.47	0.020
Right pSTG-left putamen	2.39	0.138
Left pSTG-right putamen	3.24	0.088
Left pSTG-left putamen**	10.59	0.004
Right putamen-left putamen**	90.19	< .001

Note. We raised the threshold level ($p < 0.5$) to enhance the sensitivity of our analysis, thereby facilitating the identification of statistical values within the CONN toolbox output.

*$p < .05$, two-tailed. **$p < .01$, two-tailed.

Table 2

ANOVA Results for Static Connectivity during Non-Beat Rhythms in Various Brain Regions

ROI pair	$F_{1,19}$	*p*-FDR
Right SMA-left SMA**	242.14	< .001
Right SMA-right pSTG**	12.10	0.003
Right SMA-left pSTG*	5.90	0.025
Right SMA-right putamen**	30.89	< .001
Right SMA-left putamen**	30.17	< .001
Left SMA-right pSTG*	7.68	0.012
Left SMA-left pSTG*	6.85	0.017
Left SMA-right putamen**	50.96	< .001
Left SMA-left putamen**	39.84	< .001
Right pSTG-left pSTG**	79.96	< .001
Right pSTG-right putamen	1.99	0.175
Right pSTG-left putamen	2.90	0.105
Left pSTG-right putamen	0.62	0.442
Left pSTG-left putamen	3.86	0.064
Right putamen-left putamen**	117.77	< .001

Note. We raised the threshold level ($p < 0.5$) to enhance the sensitivity of our analysis, thereby facilitating the identification of statistical values within the CONN toolbox output.

*$p < .05$, two-tailed. **$p < .01$, two-tailed.

Table 3

ANOVA Results for Static Connectivity during Silence Rhythms in Various Brain Regions

ROI pair	$F_{1,19}$	p-FDR
Right SMA-left SMA**	218.41	< .001
Right SMA-right pSTG**	11.13	0.003
Right SMA-left pSTG	2.59	0.124
Right SMA-right putamen**	53.52	< .001
Right SMA-left putamen**	28.21	< .001
Left SMA-right pSTG	4.32	0.051
Left SMA-left pSTG	2.83	0.109
Left SMA-right putamen**	73.38	< .001
Left SMA-left putamen**	40.44	< .001
Right pSTG-left pSTG**	68.61	< .001
Right pSTG-right putamen	4.28	0.052
Right pSTG-left putamen	0.30	0.590
Left pSTG-right putamen	0.51	0.483
Left pSTG-left putamen	0.84	0.372
Right putamen-left putamen**	112.04	< .001

Note. We raised the threshold level ($p < 1$) to enhance the sensitivity of our analysis, thereby facilitating the identification of statistical values within the CONN toolbox output.

*$p < .05$, two-tailed. **$p < .01$, two-tailed.

Table 4

ANOVA Results Representing the Effect of Stimulus Type on Static Connectivity Differences in Various Brain Regions

ROI pair	$F_{2,19}$	*p*-FDR
Right SMA-left SMA	0.02	0.982
Right SMA-right pSTG	0.28	0.761
Right SMA-left pSTG	1.30	0.298
Right SMA-right putamen	0.54	0.592
Right SMA-left putamen	0.67	0.524
Left SMA-right pSTG	0.81	0.461
Left SMA-left pSTG	0.53	0.603
Left SMA-right putamen	1.14	0.341
Left SMA-left putamen	2.96	0.077
Right pSTG-left pSTG	0.75	0.487
Right pSTG-right putamen	0.10	0.910
Right pSTG-left putamen	1.47	0.256
Left pSTG-right putamen	0.36	0.704
Left pSTG-left putamen	1.40	0.272
Right putamen-left putamen	1.93	0.174

Note. We raised the threshold level ($p < 1.0$) to enhance the sensitivity of our analysis, thereby facilitating the identification of statistical values within the CONN toolbox output.

Table 5

ANOVA Results Representing the Effect of Both Stimulus Type and Time on Functional Connectivity Differences in Various Brain Regions

	Stimulus		Time		Stimulus x Time	
ROI pair	$F_{2,38}$	p	$F_{8,152}$	p	$F_{16,304}$	p
Right SMA-left SMA	0.04	0.961	1.05	0.402	0.69	0.808
Right SMA-right pSTG	0.38	0.687	0.13	0.998	0.53	0.929
Right SMA-left pSTG	1.13	0.333	0.12	0.998	1.14	0.319
Right SMA-right putamen	0.44	0.649	0.42	0.910	1.13	0.322
Right SMA-left putamen	0.79	0.460	0.18	0.993	1.28	0.205
Left SMA-right pSTG	0.21	0.812	0.09	0.999	0.57	0.904
Left SMA-left pSTG	0.58	0.565	0.27	0.976	1.43	0.127
Left SMA-right putamen	1.10	0.343	0.31	0.960	0.64	0.800
Left SMA-left putamen**	2.53	0.093	0.57	0.802	2.49	0.001
Right pSTG-left pSTG**	1.16	0.323	1.15	0.332	3.02	< .001
Right pSTG-right putamen**	0.10	0.905	1.08	0.380	3.11	< .001
Right pSTG-left putamen**	1.69	0.198	0.58	0.790	2.15	0.007
Left pSTG-right putamen	0.10	0.903	0.66	0.729	1.41	0.136
Left pSTG-left putamen	0.52	0.600	1.03	0.414	1.27	0.215
Right putamen-left putamen	1.83	0.175	0.92	0.503	1.22	0.252

*$p < .05$, two-tailed. **$p < .01$, two-tailed.

Table 6

Post-hoc Comparing Connectivity of Left Putamen and Left SMA across Time and Stimuli

Strong-beat versus Non-beat						
			M		*SD*	
Time	*t*(19)	*p*	Strong-beat	Non-beat	Strong-beat	Non-beat
Window 1	-0.26	0.798	0.27	0.29	0.32	0.34
Window 2	-1.09	0.291	0.23	0.32	0.31	0.30
Window 3	-1.69	0.107	0.19	0.32	0.31	0.31
Window 4	-1.06	0.301	0.22	0.31	0.31	0.30
Window 5	-1.48	0.156	0.18	0.3	0.29	0.29
Window 6	-1.01	0.327	0.19	0.29	0.29	0.37
Window 7	-1.33	0.200	0.17	0.32	0.31	0.37
Window 8	-2.16*	0.043	0.09	0.31	0.36	0.25
Window 9	-2.00	0.060	0.12	0.34	0.33	0.30
Strong-beat versus Silence						
			M		*SD*	
Time	*t*(19)	*p*	Strong-beat	Silence	Strong-beat	Silence
Window 1	0.18	0.862	0.27	0.25	0.32	0.36
Window 2	0.55	0.586	0.23	0.18	0.31	0.33
Window 3	0.18	0.863	0.19	0.17	0.31	0.35
Window 4	0.27	0.787	0.22	0.19	0.31	0.33
Window 5	-0.69	0.500	0.18	0.24	0.29	0.27
Window 6	-3.48**	0.003	0.19	0.37	0.29	0.23
Window 7	-3.22**	0.005	0.17	0.39	0.31	0.26
Window 8	-3.08**	0.006	0.09	0.4	0.36	0.33
Window 9	-2.94**	0.008	0.12	0.39	0.33	0.28
Non-beat versus Silence						
			M		*SD*	
Time	*t*(19)	*p*	Non-beat	Silence	Non-beat	Silence
Window 1	0.51	0.616	0.29	0.25	0.34	0.36
Window 2	1.90	0.073	0.32	0.18	0.30	0.33
Window 3	1.78	0.091	0.32	0.17	0.31	0.35
Window 4	1.29	0.213	0.31	0.19	0.30	0.33
Window 5	0.80	0.435	0.30	0.24	0.29	0.27
Window 6	-1.04	0.310	0.29	0.37	0.37	0.23
Window 7	-0.72	0.482	0.32	0.39	0.37	0.26
Window 8	-1.13	0.274	0.31	0.40	0.25	0.33
Window 9	-0.62	0.543	0.34	0.39	0.30	0.28

Note. The means represent Fisher-transformed bivariate correlation coefficients.

*$p < .05$, two-tailed. **$p < .01$, two-tailed.

Table 7

Post-hoc Comparing Connectivity of Right pSTG and Left Putamen across Time and Stimuli

Strong-beat versus Non-beat						
			M		*SD*	
Time	*t*(19)	*p*	Strong-beat	Non-beat	Strong-beat	Non-beat
Window 1	0.93	0.366	0.14	0.06	0.29	0.28
Window 2	1.03	0.314	0.17	0.09	0.27	0.26
Window 3	-0.21	0.838	0.11	0.12	0.29	0.23
Window 4	0.53	0.606	0.10	0.08	0.24	0.23
Window 5	-0.55	0.587	0.07	0.10	0.22	0.28
Window 6	-1.82	0.084	-0.02	0.10	0.21	0.34
Window 7	-1.34	0.195	-0.02	0.09	0.22	0.33
Window 8	-1.90	0.073	-0.06	0.12	0.31	0.39
Window 9	-1.56	0.136	-0.05	0.10	0.29	0.35
Strong-beat versus Silence						
			M		*SD*	
Time	*t*(19)	*p*	Strong-beat	Silence	Strong-beat	Silence
Window 1	0.84	0.411	0.14	0.06	0.29	0.32
Window 2	2.23*	0.038	0.17	-0.04	0.27	0.27
Window 3	1.90	0.073	0.11	-0.07	0.29	0.27
Window 4	2.39*	0.028	0.10	-0.10	0.24	0.31
Window 5	1.60	0.126	0.07	-0.08	0.22	0.32
Window 6	-0.21	0.838	-0.02	0.00	0.21	0.33
Window 7	-0.58	0.567	-0.02	0.04	0.22	0.39
Window 8	-1.20	0.244	-0.06	0.07	0.31	0.29
Window 9	-1.08	0.293	-0.05	0.04	0.29	0.24
Non-beat versus Silence						
			M		*SD*	
Time	*t*(19)	*p*	Non-beat	Silence	Non-beat	Silence
Window 1	0.03	0.980	0.06	0.06	0.28	0.32
Window 2	1.52	0.146	0.09	-0.04	0.26	0.27
Window 3	2.57*	0.019	0.12	-0.07	0.23	0.27
Window 4	2.66*	0.016	0.08	-0.10	0.23	0.31
Window 5	1.98	0.062	0.10	-0.08	0.28	0.32
Window 6	1.06	0.305	0.10	0.00	0.34	0.33
Window 7	0.47	0.647	0.09	0.04	0.33	0.39
Window 8	0.45	0.661	0.12	0.07	0.39	0.29
Window 9	0.62	0.541	0.10	0.04	0.35	0.24

Note. The means represent Fisher-transformed bivariate correlation coefficients.

*$p < .05$, two-tailed. **$p < .01$, two-tailed.

Table 8

Post-hoc Comparing Connectivity of Right pSTG and Left pSTG across Time and Stimuli

Strong-beat versus Non-beat						
			M		*SD*	
Time	*t*(19)	*p*	Strong-beat	Non-beat	Strong-beat	Non-beat
Window 1	-0.14	0.889	0.69	0.71	0.35	0.35
Window 2	0.62	0.541	0.78	0.72	0.35	0.36
Window 3	-0.21	0.833	0.83	0.85	0.39	0.44
Window 4	0.57	0.574	0.84	0.77	0.39	0.52
Window 5	1.25	0.225	0.86	0.72	0.43	0.48
Window 6	0.62	0.543	0.81	0.72	0.47	0.48
Window 7	0.24	0.816	0.68	0.65	0.44	0.39
Window 8	0.55	0.591	0.68	0.62	0.40	0.41
Window 9	-0.78	0.447	0.57	0.65	0.40	0.39
Strong-beat versus Silence						
			M		*SD*	
Time	*t*(19)	*p*	Strong-beat	Silence	Strong-beat	Silence
Window 1	1.26	0.222	0.69	0.55	0.35	0.38
Window 2	2.35*	0.030	0.78	0.50	0.35	0.38
Window 3	2.42*	0.026	0.83	0.55	0.39	0.39
Window 4	2.07	0.053	0.84	0.60	0.39	0.37
Window 5	2.07	0.052	0.86	0.59	0.43	0.45
Window 6	1.40	0.179	0.81	0.63	0.47	0.44
Window 7	0.16	0.872	0.68	0.66	0.44	0.42
Window 8	-0.07	0.949	0.68	0.69	0.40	0.49
Window 9	-1.32	0.203	0.57	0.76	0.40	0.45
Non-beat versus Silence						
			M		*SD*	
Time	*t*(19)	*p*	Non-beat	Silence	Non-beat	Silence
Window 1	1.52	0.144	0.71	0.55	0.35	0.38
Window 2	2.54*	0.020	0.72	0.50	0.36	0.38
Window 3	3.13**	0.006	0.85	0.55	0.44	0.39
Window 4	1.78	0.091	0.77	0.60	0.52	0.37
Window 5	1.23	0.233	0.72	0.59	0.48	0.45
Window 6	0.89	0.386	0.72	0.63	0.48	0.44
Window 7	-0.11	0.912	0.65	0.66	0.39	0.42
Window 8	-0.60	0.553	0.62	0.69	0.41	0.49
Window 9	-0.96	0.348	0.65	0.76	0.39	0.45

Note. The means represent Fisher-transformed bivariate correlation coefficients.

*$p < .05$, two-tailed. **$p < .01$, two-tailed.

Table 9

Post-hoc Comparing Connectivity of Right pSTG and Right Putamen across Time and Stimuli

Strong-beat versus Non-beat						
			M		*SD*	
Time	*t*(19)	*p*	Strong-beat	Non-beat	Strong-beat	Non-beat
Window 1	2.15*	0.045	0.21	0.02	0.29	0.34
Window 2	2.76*	0.013	0.24	0.06	0.25	0.29
Window 3	2.07	0.053	0.18	0.07	0.27	0.21
Window 4	0.35	0.731	0.10	0.08	0.20	0.21
Window 5	-0.78	0.445	0.07	0.11	0.16	0.26
Window 6	-2.36*	0.029	0.01	0.16	0.17	0.30
Window 7	-1.94	0.068	-0.02	0.14	0.21	0.29
Window 8	-1.63	0.120	-0.08	0.08	0.31	0.35
Window 9	-1.26	0.223	-0.08	0.06	0.35	0.37
Strong-beat versus Silence						
			M		*SD*	
Time	*t*(19)	*p*	Strong-beat	Silence	Strong-beat	Silence
Window 1	2.15*	0.045	0.21	0.03	0.29	0.24
Window 2	3.27**	0.004	0.24	0.03	0.25	0.20
Window 3	2.23*	0.038	0.18	0.03	0.27	0.20
Window 4	0.16	0.874	0.10	0.09	0.20	0.24
Window 5	-0.41	0.686	0.07	0.10	0.16	0.25
Window 6	-1.89	0.074	0.01	0.14	0.17	0.26
Window 7	-2.06	0.053	-0.02	0.14	0.21	0.28
Window 8	-2.10*	0.050	-0.08	0.12	0.31	0.24
Window 9	-1.71	0.103	-0.08	0.09	0.35	0.23
Non-beat versus Silence						
			M		*SD*	
Time	*t*(19)	*p*	Non-beat	Silence	Non-beat	Silence
Window 1	-0.08	0.941	0.02	0.03	0.34	0.24
Window 2	0.33	0.745	0.06	0.03	0.29	0.20
Window 3	0.67	0.510	0.07	0.03	0.21	0.20
Window 4	-0.07	0.943	0.08	0.09	0.21	0.24
Window 5	0.16	0.875	0.11	0.10	0.26	0.25
Window 6	0.19	0.851	0.16	0.14	0.30	0.26
Window 7	-0.02	0.982	0.14	0.14	0.29	0.28
Window 8	-0.38	0.708	0.08	0.12	0.35	0.24
Window 9	-0.29	0.778	0.06	0.09	0.37	0.23

Note. The means represent Fisher-transformed bivariate correlation coefficients.

*$p < .05$, two-tailed. **$p < .01$, two-tailed.

Figures

Figure 1

Temporal Dynamics of ROI-ROI Functional Connectivity Patterns

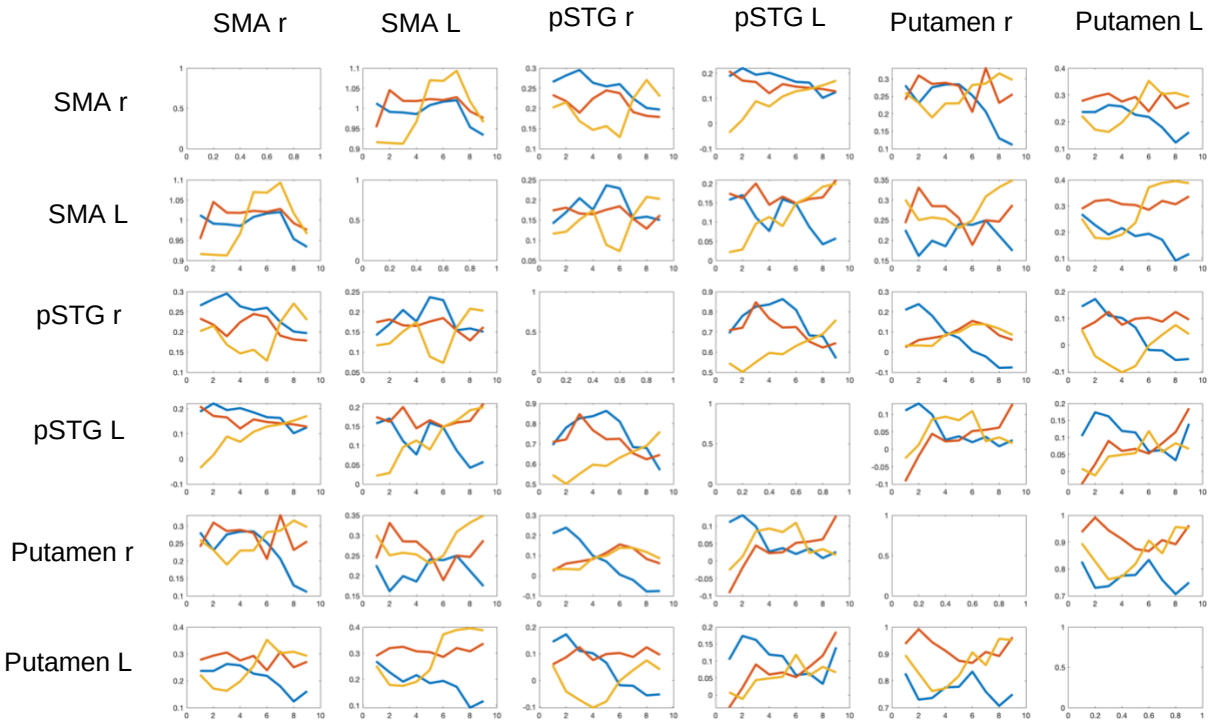

Note. The x-axis represents the time windows, and the y-axis represents the Fisher-transformed bivariate correlation coefficients of the functional connectivity in the corresponding regions. Blue represents the strong-beat condition, red represents the non-beat condition, and yellow represents the silence condition.

Figure 2

Temporal Dynamics of Left SMA and Left Putamen Functional Connectivity

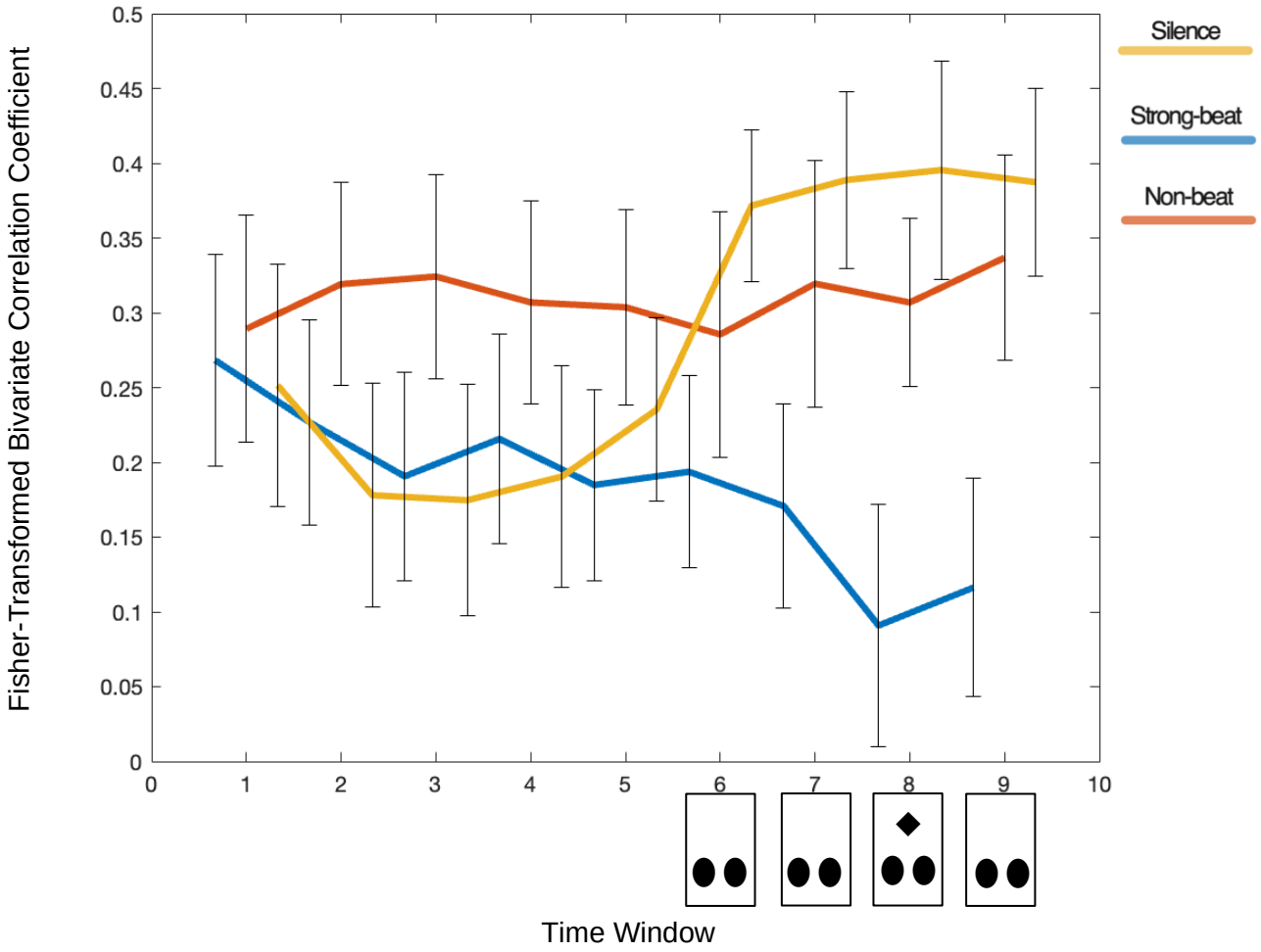

Note. Fisher-Transformed bivariate correlations represent functional connectivity measures. Geometrical shapes represent the statistical significance for different time windows being compared via the post-hoc t-test.

◆$p < .05$, two-tailed. ◆◆$p < .01$, two-tailed. (Strong-beat versus non-beat)

●$p < .05$, two-tailed. ●●$p < .01$, two-tailed. (Strong-beat versus silence)

★$p < .05$, two-tailed. ★★$p < .01$, two-tailed. (Non-beat versus silence)

Figure 3

Temporal Dynamics of Right pSTG and Left Putamen Functional Connectivity

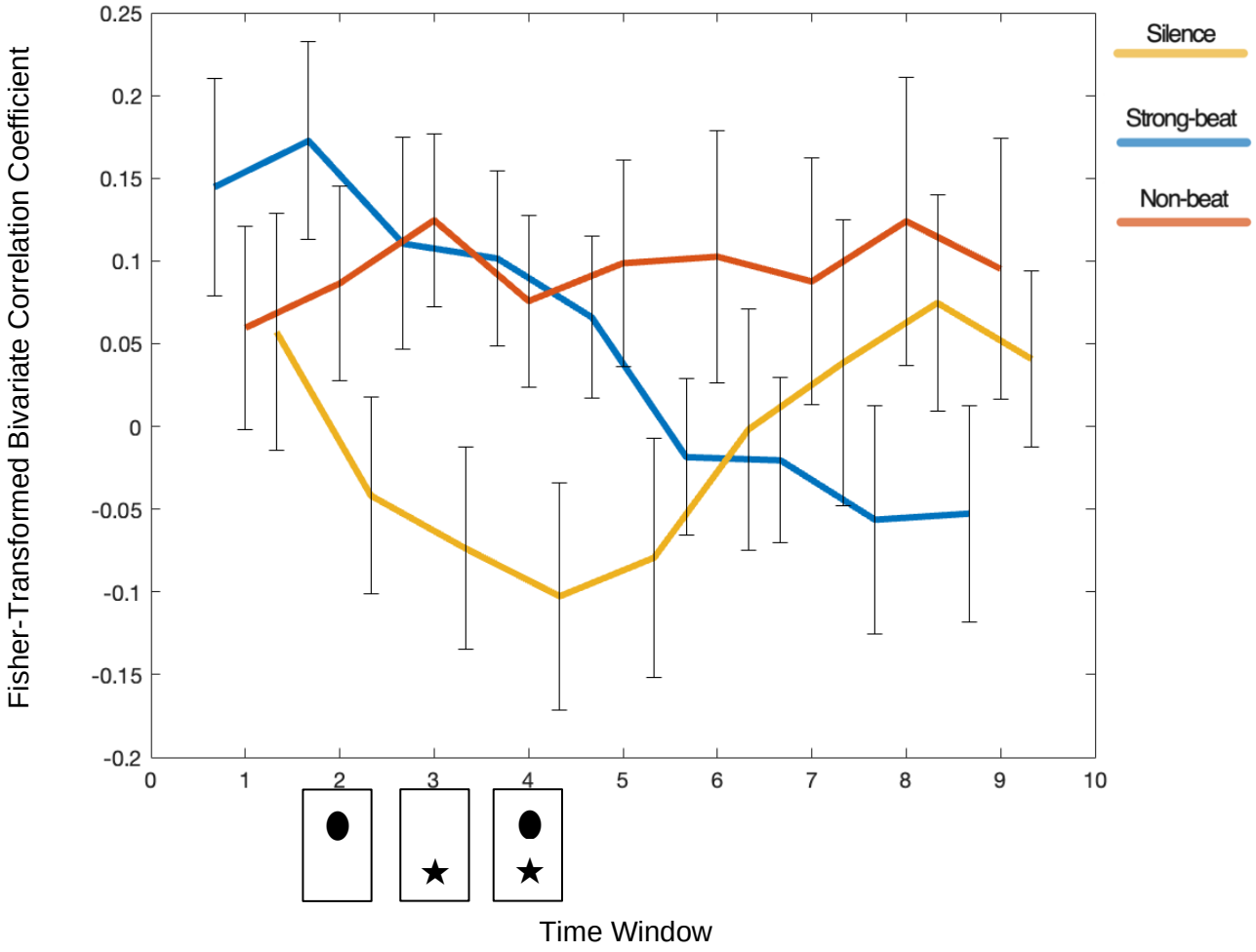

Note. Fisher-transformed bivariate correlations represent functional connectivity measures. Geometrical shapes represent the statistical significance for different time windows being compared via the post-hoc t-test.

◆$p < .05$, two-tailed. ◆◆$p < .01$, two-tailed. (Strong-beat versus non-beat)

●$p < .05$, two-tailed. ●●$p < .01$, two-tailed. (Strong-beat versus silence)

★$p < .05$, two-tailed. ★★$p < .01$, two-tailed. (Non-beat versus silence)

Figure 4

Temporal Dynamics of Right pSTG and Left pSTG Functional Connectivity

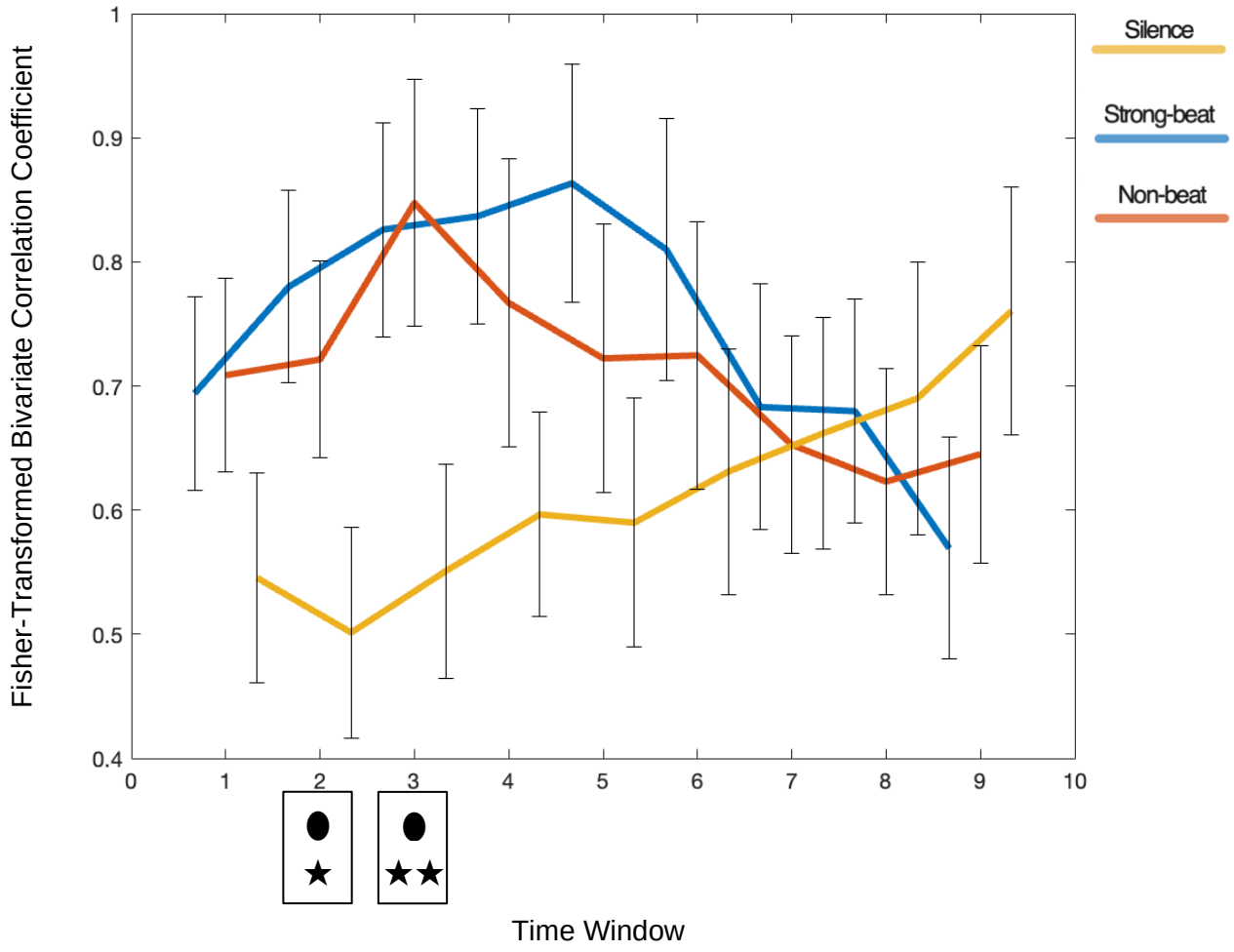

Note. Fisher-transformed bivariate correlations represent functional connectivity measures. Geometrical shapes represent the statistical significance for different time windows being compared via the post-hoc t-test.

◆$p < .05$, two-tailed. ◆◆$p < .01$, two-tailed. (Strong-beat versus non-beat)

●$p < .05$, two-tailed. ●●$p < .01$, two-tailed. (Strong-beat versus silence)

★$p < .05$, two-tailed. ★★$p < .01$, two-tailed. (Non-beat versus silence)

Figure 5

Temporal Dynamics of Right pSTG and Right Putamen Functional Connectivity

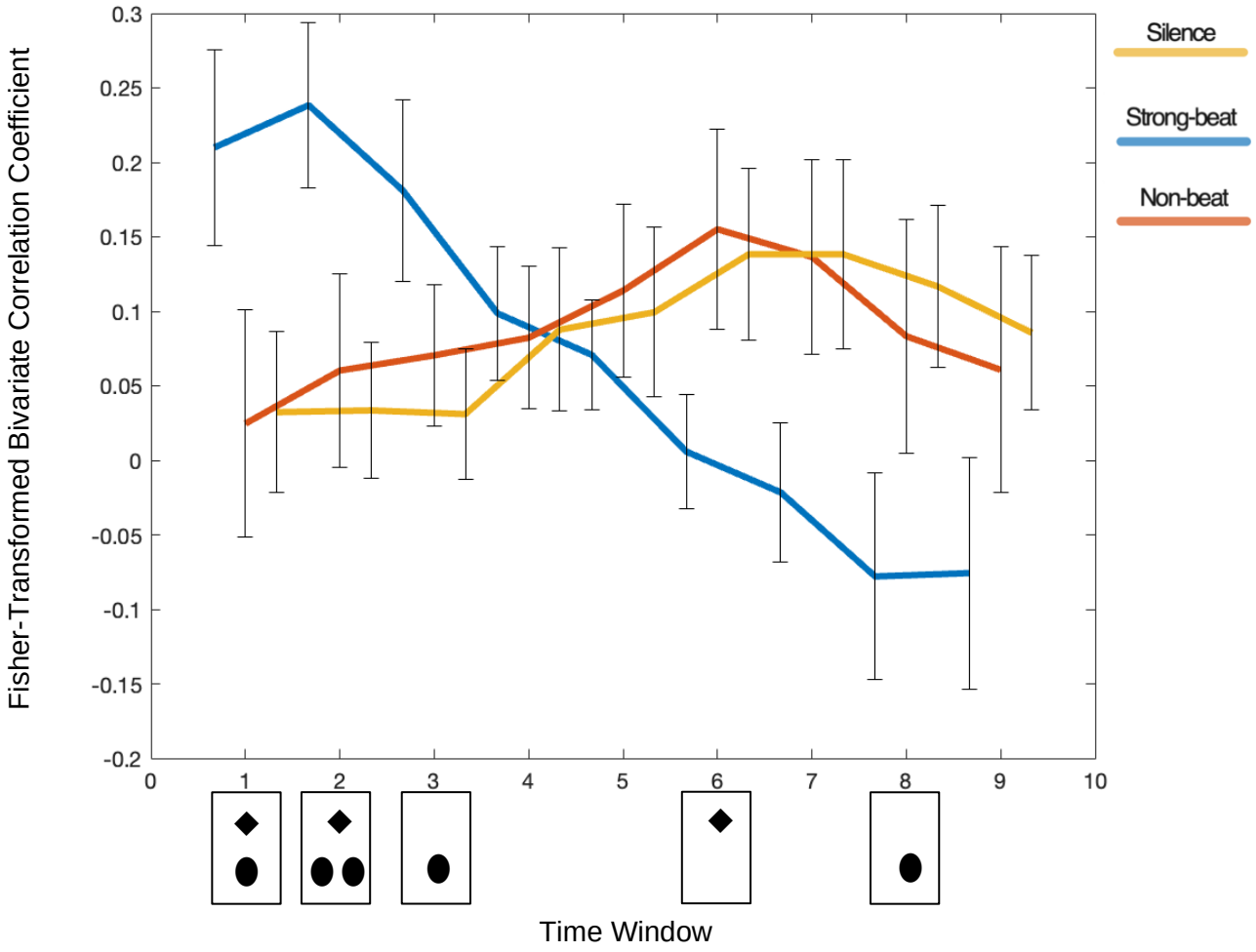

Note. Fisher-transformed bivariate correlations represent functional connectivity measures. Geometrical shapes represent the statistical significance for different time windows being compared via the post-hoc t-test.

◆$p < .05$, two-tailed. ◆◆$p < .01$, two-tailed. (Strong-beat versus non-beat)

●$p < .05$, two-tailed. ●●$p < .01$, two-tailed. (Strong-beat versus silence)

★$p < .05$, two-tailed. ★★$p < .01$, two-tailed. (Non-beat versus silence)